Published August 12, 2013

Q/R site interactions with the M3 helix in GluK2 kainate receptor channels revealed by thermodynamic mutant cycles

Melany N. Lopez, Timothy J. Wilding, and James E. Huettner

Department of Cell Biology and Physiology, Washington University School of Medicine in St. Louis, St. Louis, MO 63110

RNA editing at the Q/R site near the apex of the pore loop of AMPA and kainate receptors controls a diverse array of channel properties, including ion selectivity and unitary conductance and susceptibility to inhibition by polyamines and cis-unsaturated fatty acids, as well as subunit assembly into tetramers and regulation by auxiliary subunits. How these different aspects of channel function are all determined by a single amino acid substitution remains poorly understood; however, several lines of evidence suggest that interaction between the pore helix (M2) and adjacent segments of the transmembrane inner (M3) and outer (M1) helices may be involved. In the present study, we have used double mutant cycle analysis to test for energetic coupling between the Q/R site residue and amino acid side chains along the M3 helix. Our results demonstrate interaction with several M3 locations and particularly strong coupling to substitution for L614 at the level of the central cavity. In this location, replacement with smaller side chains completely and selectively reverses the effect of fatty acids on gating of edited channels, converting strong inhibition of wild-type GluK2(R) to nearly 10-fold potentiation of GluK2(R) L614A.

INTRODUCTION

Ionotropic glutamate receptors (iGluRs) are members of the pore loop superfamily of ion channels in which four subunits, or in some cases linked pseudo-subunits, generate a conducting pathway for ions through the membrane (Hille, 2001). Each of the subunits contributes a reentrant loop between two transmembrane helices (M1 and M3) that combine to make up the pore. The reentrant loops include a short α helical domain (M2; ∼15 amino acids) followed by a segment of open coil that forms the narrowest section of the pore and connects to the inner transmembrane helix (M3), which lines the pore the rest of the way through the membrane (Doyle et al., 1998). All eukaryotic iGluR subunits include an additional transmembrane helix (M4) that is required for channel function (Schorge and Colquhoun, 2003; Terhag et al., 2010; Salussolia et al., 2011). In most superfamily members, the pore loop is located on the extracellular side and the inner helix bundle crossing, which is thought to form the gate for ion passage, faces the cytoplasm. However, iGluRs exhibit an inverted topology with the pore loop on the cytoplasmic side and the inner and outer helices connected to large extracellular domains that include the agonist-binding sites (Traynelis et al., 2010; Mayer, 2011).

For two of the iGluR subtypes, named for the agonists 2-amino-3-hydroxy-5-methyl-4-isoxazolepropionic acid (AMPA) and kainate (KA), several channel properties are controlled by RNA editing (Sommer et al., 1991), which enzymatically changes the coding for an amino acid located near the apex of the pore loop just past the end of the pore helix (Rosenthal and Seeburg, 2012). Editing converts the sequence for glutamine (Q) in genomic DNA to a modified codon recognized by the tRNA for arginine (R). Channels that only include unedited (Q) subunits are more permeable to calcium (Burnashev et al., 1992; Dingledine et al., 1992), exhibit voltage-dependent block of outward current by cytoplasmic polyamines (Bowie and Mayer, 1995; Kamboj et al., 1995; Koh et al., 1995), and display higher single channel conductance (Howe, 1996; Swanson et al., 1996). In addition, recombinant KA receptor channels in which all subunits are edited (R) exhibit finite permeability to chloride as well as monovalent cations (P_{Cl}/P_{Cs} ∼0.74; Burnashev et al., 1996) and display strong inhibition by cis-unsaturated fatty acids, such as arachidonic and docosahexaenoic acid (AA and DHA, respectively; Wilding et al., 2005). Finally, Q to R editing controls regulation of AMPA receptor properties by several members of the TARP auxiliary subunit family (Körber et al., 2007; Kato et al., 2008) and strongly inhibits assembly of homomeric GluA2(R) AMPA receptors (Greger et al., 2003) but not homomeric GluK2(R) KA receptors (Ma-Högemeier et al., 2010). Perhaps surprisingly, the change from Q to R has little effect on the

Correspondence to James E. Huettner: jhuettner@wustl.edu

Abbreviations used in this paper: AA, arachidonic acid; AMPA, 2-amino-3-hydroxy-5-methyl-4-isoxazolepropionic acid; Con A, concanavalin A; DHA, docosahexaenoic acid; iGluR, ionotropic glutamate receptor; KA, kainate; TMD, transmembrane domain.

The Rockefeller University Press $30.00
J. Gen. Physiol. Vol. 142 No. 3 225–239
www.jgp.org/cgi/doi/10.1085/jgp.201311000

Supplemental Material can be found at:
http://jgp.rupress.org/content/suppl/2013/08/08/jgp.201311000.DC1.html

Published August 12, 2013

minimal pore diameters of KA receptor channels, which have been estimated from the relative permeability of organic cations to be 7.5 and 7.6 Å for homomeric channels made up of GluK2 subunits in the Q or R forms, respectively (Burnashev et al., 1996). Thus, editing appears to change energetic barriers to permeation without physically constricting the pore.

Our recent work (Wilding et al., 2008, 2010) suggests that interactions between the pore loop and adjacent M1 and M3 helices may be an important determinant for gating, permeability, and susceptibility to modulation for KA receptor channels. To test this hypothesis directly, we have begun to use mutant cycle analysis (Carter et al., 1984; Hidalgo and MacKinnon, 1995) to evaluate quantitatively the energetics of interactions between residues located in M2 with those in M1 or M3. In addition, we test whether exposure to DHA changes the strength of these interactions, which provides information about how the presence of free DHA may alter the channel conformation. Mutant cycle analysis involves systematically replacing pairs of amino acids and determining whether the resulting change in channel function is larger or smaller than predicted by the sum of each substitution alone (Carter et al., 1984; Schreiber and Fersht, 1995). Additional information can be gained by swapping the position of two residues presumed to interact. Local conformational effects induced by amino acid substitution should strongly depend on the specific characteristics of the substituted residue at each position, whereas interactions between the two substituted residues may be possible in either orientation. For example, a salt bridge may be preserved by swapping the two residues (Kollewe et al., 2009), whereas the bridge will be disrupted by substitution for either residue individually. Strong and specific compensation such as this provides evidence for a direct interaction between the two residues. More distant residues may still exhibit either synergy or compensation, but the coupling will typically be weaker than 1.5 *k*T (Schreiber and Fersht, 1995) and less dependent on the specific identity of the replacing side chain, suggesting a more global change in protein conformation or through space electrostatic compensation (Chatelain et al., 2005). Ideally, the method should provide a quantitative measure of pairwise interactions between amino acid residues.

In the present study, we have used double mutant cycle analysis to evaluate the strength of interactions between the Q/R site at the apex of the pore loop and residues along the M3 transmembrane helix. Our results from analysis of polyamine block and channel modulation by DHA provide evidence for interactions in the open state between the Q/R site residue and the amino acid side chain at M3 position 614, despite a predicted separation of more than 8–12 Å in the closed state.

MATERIALS AND METHODS

cDNA, cell culture, and transfection

M. Mayer (National Institutes of Health, Bethesda, MD) provided a GluK2 cDNA construct (Panchenko et al., 1999) in the pRK5 expression vector that includes three novel silent restriction sites engineered in sequences encoding the M1 helix (NheI), the beginning of the M3 helix (MluI), and in the S2 region (BglII) downstream of M3. Site-directed mutations were generated by PCR using a mutation primer that spanned one of these novel restriction sites or the endogenous unique Bstz17I site in M3. PCR products and GluK2 were cut with the appropriate enzymes, purified, and ligated. All constructs were sequenced through the entire ligated segment by the Washington University in St. Louis Protein and Nucleic Acid Chemistry Laboratory to verify the mutation and correct restriction joints. cDNAs were expressed by transient transfection of HEK 293 cells. The HEK cells were maintained in 25-mm^2 flasks and passaged weekly using protease XXIII. Cells for transfection were seeded into 12-well plates and the next day incubated with a mixture of 1–3 µg of subunit cDNA, 1 µg cDNA encoding GFP (pEGFP; Takara Bio Inc.), and Lipofectamine 2000 according to the manufacturer's protocol. The day after transfection, cells were transferred to nitrocellulose coated in 35-mm dishes, and recordings were obtained 1–2 d later from transfected cells identified by epi-illumination.

Electrophysiology

Culture dishes were perfused continuously with Tyrode's solution (in mM): 150 NaCl, 4 KCl, 2 $MgCl_2$, 2 $CaCl_2$, 10 glucose, and 10 HEPES, pH 7.4 with NaOH. Electrodes contained an internal solution of (in mM) 140 Cs glucuronate, 10 EGTA, 5 CsCl, 5 $MgCl_2$, 5 ATP, 1 GTP, 0.02 spermine, and 10 HEPES, pH adjusted to 7.4 with CsOH, and had an open tip resistance of 2–4 MΩ. An Axopatch 200A amplifier recorded currents, which were filtered at 1 kHz (−3 dB, 4 pole Bessel), and digitized at 5–10 kHz. For most experiments, steady-state agonist responses were increased by pretreating the cells with 2 µM concanavalin A (Con A; Huettner, 1990). A gravity-fed eight-barreled local perfusion pipette delivered control and agonist-containing extracellular solutions (160 NaCl, 10 HEPES, and 2 $CaCl_2$, pH to 7.4 with NaOH) to the cells during most recordings. For rapid extracellular exchange, the solution reservoirs were maintained under ∼10 p.s.i. static air pressure, and flow was controlled by computer-operated electronic valves as described previously (Wilding et al., 2008). As previously described (Wilding et al., 2010), a low chloride extracellular solution was used to test for chloride permeability (160 Na glucuronate, 10 HEPES, and 2 $CaCl_2$, pH to 7.4 with NaOH). Membrane potentials were corrected for a junction potential of −10 mV between the internal solution and Tyrode's solution in which seals were formed.

Analysis

I-V relations were recorded using a triangle wave stimulus to ramp the membrane potential from −160 to 110 mV at 0.75 mV/ms. Means of five ramps repeated in control solution immediately before or after exposure to KA were subtracted from the mean ramp current during KA application (Fig. S1, A–C). In most experiments, there was little or no hysteresis between rising and descending ramps, thus interaction with polyamines was assumed to be at steady-state (Rozov et al., 1998). In the present study, we did not use voltage jumps or ultrafast solution changes that would be needed to resolve changes in polyamine block of closed channels (Bowie et al., 1998; Rozov et al., 1998). Chord conductance was calculated from $G = I/(V_m - V_{rev})$, where I is whole-cell current, V_m the membrane potential, and V_{rev} the reversal potential. The coupling coefficient Ω for polyamine block was calculated from the following equation (Hidalgo and MacKinnon, 1995):

Published August 12, 2013

$\Omega = (K_{d\ WT:WT} \times K_{d\ mut1:mut2})/(K_{d\ mut1:WT} \times K_{d\ WT:mut2})$, where K_d was determined at 0 mV from normalized conductance-voltage plots fit with an equation describing a voltage-dependent permeant blocker (Fig. S1; Panchenko et al., 1999, 2001; Wilding et al., 2010): $G = 1/(1 + (1/B))$, where $B = \exp(-(V_m - V_b)/k_b) + \exp((V_m - V_p)/k_p)$, where V_b, V_p, k_b, and k_p are the midpoint voltages and slope factors for polyamine block and permeation, respectively. Polyamine K_d at 0 mV was calculated as $K_{d(0)} = [\text{spermine}] \times (\exp(V_b/k_b) + \exp(-V_p/k_p))$. Coupling energies were calculated from $\Delta G = kT \ln\Omega$, where k is Boltzmann's constant and T is the absolute temperature (273.15 + °C).

Current fluctuations were analyzed as described previously (Huettner, 1990; Wilding et al., 2008) using data recorded during slow bath application of 10 µM KA in the presence or absence of 15 µM DHA (Fig. S2). Steady-state current variance was calculated over 100-ms time intervals after correcting for steady amplitude changes by subtracting a straight line fit. Variance (σ^2) versus mean current (I) plots were fit with the parabolic equation $\sigma^2 = i \times I - I^2/N$, where i is the estimated unitary current amplitude and N the estimated number of channels (Sigworth, 1980). Maximal open probability was estimated from $P_o = I_{max}/(i \times N)$, and exposure to DHA was assumed not to change the number of channels (N). When P_o is less than ~0.2, the variance versus mean plot is approximately linear with slope equal to the unitary current (i). Therefore, for cells with $P_o < 0.4$ (17 out of 81 cells analyzed), we calculated the ratio of residual deviations (Swartz et al., 1992) to test whether there was statistical justification to use the two-parameter parabolic function instead of the best-fit straight line through the origin with the slope as the only free parameter (Fig. S2). In 8 of the 17 cells, the parabolic fit was significantly superior and the estimated P_o was >0.25, consistent with a previous simulation study suggesting that reliable estimates can be obtained for P_o as low as 0.2 (Lingle, 2006). For the remaining nine cells, we assumed a maximal P_o of 0.2 and calculated the P_o in DHA or control solution relative to that value. Importantly, for all of the constructs analyzed, we had several cells with P_o of at least 0.4 or greater.

To compare the action of DHA on mutant (mut) and WT receptors, we calculated the change in free energy (ΔG) from estimated open probability (P_o): $\Delta G = -RT\ln K_{eq}$, where $K_{eq} = P_o/(1 - P_o)$ and for individual mutations $\Delta\Delta G = \Delta G_{mut} - \Delta G_{WT} = (\Delta G_{mut}^{DHA} - \Delta G_{mut}) - (\Delta G_{WT}^{DHA} - \Delta G_{WT})$. Coupling coefficients for M3 helix mutations with Q/R site editing were calculated from K_{eq} values, determined both in the absence and presence of DHA, as follows: $\Omega = (K_{eq\ WT:WT} \times K_{eq\ mut1:mut2})/(K_{eq\ mut1:WT} \times K_{eq\ WT:mut2})$. All results are presented as mean ± SEM unless otherwise stated. Statistical significance was assigned at $P < 0.05$ for comparison of currents in control and DHA-containing solutions (*t* test).

Molecular modeling

Homology modeling of GluK2(R) began with our earlier model of the GluK2(Q) homotetramer (Wilding et al., 2010), which was based on the GluA2 crystal structure using the alignment in Fig. S2 of Sobolevsky et al. (2009) with a twofold symmetry constraint for the A/C and B/D subunits. For the present study, the high resolution discrete optimized protein energy (DOPE-HR) method (Shen and Sali, 2006), a component of the Modeller software package (release 9v7; Eswar et al., 2008), was used to refine the A/C and B/D M2-M3 loops with Arg at the Q/R site.

Online supplemental material

Fig. S1 illustrates the lack of hysteresis in KA-evoked current for slow ascending and descending voltage ramps and the analysis of polyamine block from conductance-voltage relations. Fig. S2 shows fluctuation analysis of KA-evoked currents for GluK2(R) L614E. Fig. S3 shows I-V relations for L614D(R) and L614R(D) mutant cycles. Fig. S4 plots coupling energies derived from analysis of polyamine block for M3 substitutions with Ala, Cys, and Val. Table S1 shows reversal potentials and estimated relative chloride permeability. Online supplemental material is available at http://www.jgp.org/cgi/content/full/jgp.201311000/DC1.

RESULTS

Previous work suggests that GluK2 channel inhibition by exposure to DHA depends on interactions along the interface between the pore loop helix and the transmembrane M1 and M3 helices (Fig. 1; Wilding et al., 2008, 2010). To gain more information about this interaction and determine which specific residues are involved, we tested for pairwise interactions between the Q/R site and a set of substitutions along the M3 helix.

M3 substitutions with charged side chains: Polyamine block

An earlier study showed that substitution with positively charged Arg residues at several locations along M3 significantly reduced the apparent affinity for polyamines (Wilding et al., 2010). To test for possible electrostatic interactions between the Q/R site and these M3 positions, we compared polyamine block for single and double mutants combining positive (arginine, R) or negative (glutamate, E; and aspartate, D) side chain substitutions. Fig. 2 A shows results for R and E substitutions at

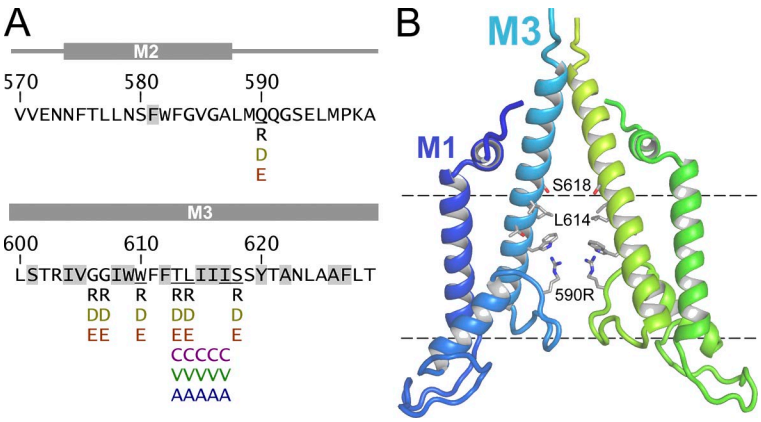

Figure 1. Location of M3 residues tested for interaction with the Q/R site. (A) Primary sequence of GluK2 from M2 through M3. Substituted residues are listed below the WT sequence. Locations where whole-cell KA-evoked currents were too small to analyze in homomeric Arg substitution mutants are shaded (Wilding et al., 2008, 2010). Gray boxes above the sequence denote putative M2 and M3 α helical domains. (B) Homology model of the M1-M3 segment of GluK2(R) A and C subunits (Wilding et al., 2010) based on the x-ray structure of the homomeric GluA2 AMPA receptor closed state (Sobolevsky et al., 2009). Side chains underlined in A are displayed including the edited (Q590R) form of the Q/R site. The region between the dashed lines is shown in Fig. 8, as viewed from above.

Published August 12, 2013

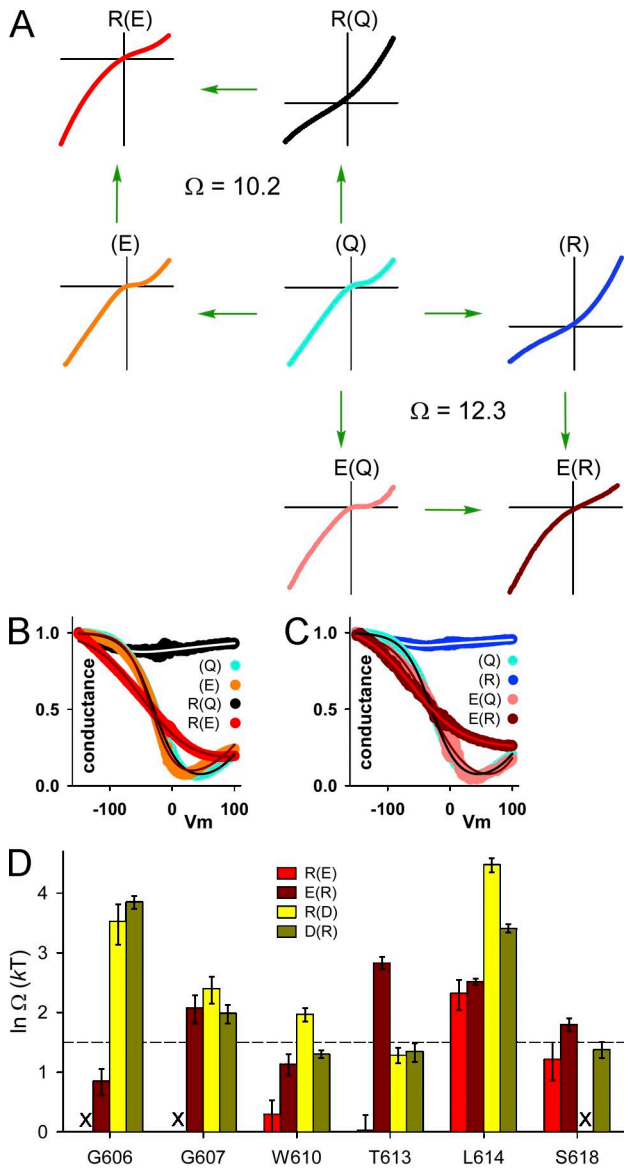

Figure 2. Coupling energies from mutant cycle analysis of polyamine block. (A) Mutant cycles for R and E substitutions at the Q/R site and at position L614 in the M3 helix. Plots show KA-evoked whole-cell current recorded for WT GluK2(Q) and (R), for GluK2(E), and for substitution mutants at position L614 between −150 and 100 mV during slow voltage ramps (0.75 mV/ms; see Fig. S1, A–C). Bi-rectification of current mediated by GluK2(Q) reflects strong block by endogenous polyamines, as well as 20 µM spermine added to the internal solution, with progressive relief of block as the polyamines permeate the channel at more positive potentials. Q/R site editing or Arg substitution at position 614 eliminates polyamine block, whereas block is partially restored for GluK2(R) L614E and GluK2(E) L614R. (B and C) Normalized conductance versus voltage plots for the constructs in A. Smooth curves are the best fits of $G = 1/(1 + (1/B))$, where $B = \exp(-(V_m - V_b)/k_b) + \exp((V_m - V_p)/k_p)$, where V_b, V_p, k_b, and k_p are the midpoint voltages and slope factors for polyamine block and permeation, respectively (see Materials and methods and Fig. S1 D). Polyamine K_d at 0 mV $K_{d(0)}$ = [spermine] × $(\exp(V_b/k_b) + \exp(-V_p/k_p))$ was used to calculate the coupling coefficients: $\Omega = (K_{d\,WT:WT} \times K_{d\,mut1:mut2})/(K_{d\,mut1:WT} \times K_{d\,WT:mut2})$. (D) Coupling energies for 21 mutant cycles were calculated as $\Delta G = kT \ln\Omega$, where k is Boltzmann's constant and T is the absolute temperature. The dashed line at 1.5 kT plots the empirical coupling energy threshold for interacting residues believed to make close contact. Results are presented as mean ± SEM.

the Q/R site and L614 in M3. As demonstrated in previous studies (Bowie and Mayer, 1995; Kamboj et al., 1995; Koh et al., 1995), WT homomeric unedited (Q) channels exhibit strong block by cytoplasmic polyamines as indicated by inward rectification up to ∼50 mV; above this voltage, outward current is restored by a progressive increase in blocker permeation through the channel (Fig. 2). Editing of Q590 to (R) inhibits polyamine block, resulting in a current voltage relation that is linear or shows slight outward rectification (Panchenko et al., 1999). The M3 L614E substitution has little effect on polyamine block as a single mutation of GluK2(Q) but partially restores block when combined with Q to R editing in GluK2(R). Similarly, substitution with (E) at the Q/R site causes relatively little change in polyamine block (see also Panchenko et al., 1999) but partially restores block when combined with L614R, a mutation in M3 that eliminates polyamine block of GluK2(Q) (Fig. 2; Wilding et al., 2010). Thus, the degree of compensation observed between the two charged residues is preserved when their M3 or pore loop locations are swapped. The strength of these interactions was determined from the coupling coefficients 10.2 and 12.3, indicating coupling energies of 2.3 and 2.5 kT for the R(E) and E(R) cycles, respectively, where the Q/R site residue is given in parenthesis.

In addition to position 614, we performed similar analysis for five other locations along M3 where our previous work had shown that Arg substitution mutants functioned as homomeric channels (Wilding et al., 2010). The plot in Fig. 2 D shows the coupling energies for 21 different pairwise combinations between the Q/R site and six positions along M3. Interestingly, both the D(R) and R(D) substitutions (Fig. 2 D, dark and light yellow bars, respectively) displayed the strongest coupling of the Q/R site with G606 and L614 but weaker coupling for locations in between. In contrast, the E(R) and R(E) substitutions (Fig. 2 D, dark and light red bars, respectively) showed less agreement at individual positions and no clear trend with distance along M3, suggesting that within a specific mutational context the longer, more flexible E side chain may adopt configurations that either enhance or reduce coupling with R. For comparison with previous work (Schreiber and Fersht, 1995; Hidalgo and MacKinnon, 1995), the dashed line at 1.5 kT in Fig. 2 D plots the empirical coupling energy threshold for interacting residues believed to make close contact (<4 Å). In our homology model based on the closed state x-ray crystal structure of homomeric GluA2 (Sobolevsky et al., 2009), a substantially larger closed state separation is

Published August 12, 2013

predicted for several of the residues with coupling energies >1.5 *k*T (e.g., 8–12 Å for L614). Thus, our results would be consistent with a significant movement of the pore loop relative to M3 when channels open. However, the experiments in Fig. 2 are not entirely conclusive because polyamines, which enter and pass through the pore, might bridge between the Q/R site and M3 locations, suggesting that the energies plotted in Fig. 2 D may represent coupling between polyamines and the two different channel residues, rather than coupling between the residues themselves. This would seem to be a particular concern for channels with a negatively charged Glu or Asp substituted at the Q/R site, which might be expected to promote entry of cytoplasmic polyamines into the narrowest region of the channel despite the presence of a positively charged residue along M3. In contrast, it should be noted that polyamine block is no stronger for GluK2(E) than for GluK2(Q) (Fig. 2 A; Panchenko et al., 1999; Wilding et al., 2008) and is actually substantially weaker for GluK2(D) (Fig. S3; Panchenko et al., 1999). Thus, inward rectification is stronger for the double mutant GluK2(D) L614R than for either of the single substitutions (Fig. S3), a result which is difficult to explain by independent interaction of polyamine with the two residues individually and instead suggests interaction between the substituted residues. Similarly, it is not clear how adding negatively charged side chains in the central cavity would facilitate polyamine block of GluK2(R) if the substituted M3 residue did not interact with and neutralize the four positively charged Arg guanidinium groups at the Q/R site (e.g., L614E(R); Fig. 2 A), which in WT edited channels are thought to preclude polyamines from ever entering the pore (see Fluctuation analysis and Discussion).

M3 substitutions with charged side chains: DHA inhibition and potentiation

In addition to polyamine block, we compared the effect of DHA application on agonist-evoked currents for homomeric GluK2 with charged amino acid substitutions in M3 (Fig. 3). In Fig. 3 B, the black bars replot our previous data (Wilding et al., 2010) for R substitutions at M3 locations of GluK2(Q). The bright red and yellow bars show that replacing Q590 with E or D, respectively, substantially reduced the action of DHA on channels with R substitutions at three of the six positions along M3. Inhibition of G607R and W610R, as well as potentiation of L614R, was reduced by E and/or D substitution at Q590 (i.e., $I_{DHA}/I_{control}$ values were closer to 1.0 than for the same M3 Arg substitutions in GluK2(Q)), whereas inhibition of G606R and T613R, as well as potentiation of S618R, was not much affected by replacement of Q590 with a negatively charged side chain. In addition, DHA inhibition of GluK2(R) was progressively relieved by D substitution at G607, W610, and T613 and converted to potentiation for D substitutions at S618 and, most prominently, at L614. In contrast, M3 substitution with the slightly longer E side chain caused much less change in DHA inhibition of GluK2(R)

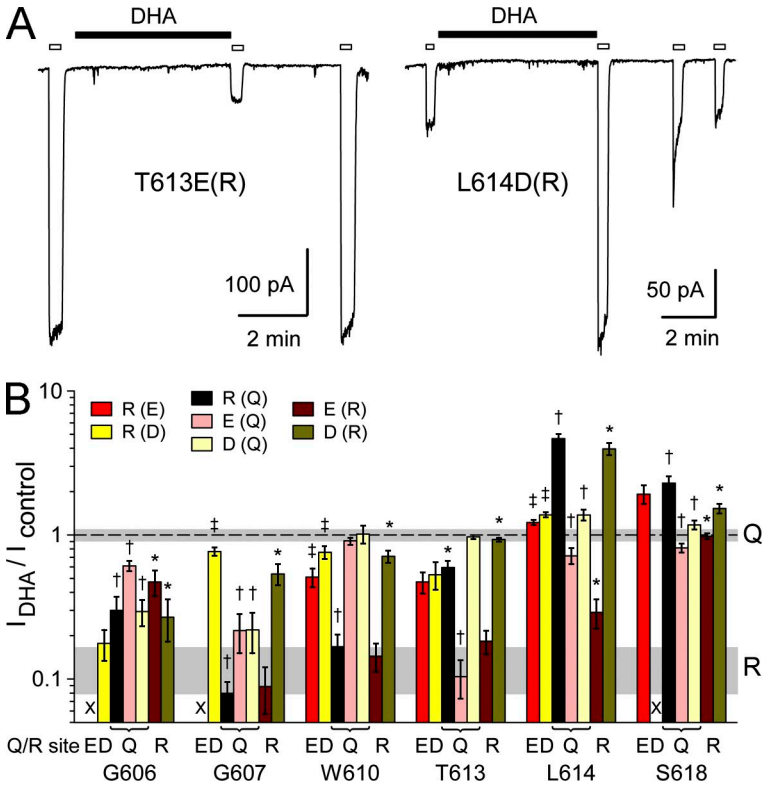

Figure 3. Charged M3 substitutions can reverse the action of DHA. (A) Whole-cell currents evoked by 10 µM KA before and after exposure to 15 µM DHA, which inhibits homomeric GluK2(R) T613E, as for WT edited GluK2(R), but potentiates current mediated by GluK2(R) L614D. (B) Plot of KA-evoked current immediately after exposure to DHA as a fraction of control current before DHA ($I_{DHA}/I_{control}$) for 40 GluK2 substitution mutants (4–48 cells for each construct). Gray horizontal bars centered on 0.12 and 1.0 indicate the 99% confidence intervals for WT GluK2(R) and (Q), respectively. Whole-cell currents mediated by G606R(E), G607R(E), and S618R(D) mutants were too small to analyze (X). Significant difference from WT GluK2(R) (*), WT GluK2(Q) (†), or from the M3 Arg substitution mutant of GluK2(Q) (‡; $P < 0.05$, *t* test) is indicated. Results are presented as mean ± SEM.

Published August 12, 2013

except at position S618, where inhibition was completely relieved. Collectively, our results in Figs. 2 and 3 provide evidence for interactions between the Q/R site residue and amino acids along the M3 helix that depend on the specific position along M3 and the side chain configuration (e.g., D vs. E).

Differences between the effects on polyamine block (Fig. 2) and DHA inhibition (Fig. 3) for each individual M3 substitution may reflect the different mechanisms by which these compounds interact with iGluRs. Cytoplasmic polyamines interact with the channel pore in both the open and closed states (Bowie et al., 1998; Rozov et al., 1998) and in the open state can be rapidly driven into, out of, or through the pore by changing the transmembrane voltage gradient. In contrast to block by polyamines, iGluR modulation by DHA typically involves a change in open probability (see below; Miller et al., 1992; Wilding et al., 2008), suggesting an effect on the conformational changes that underlie gating. Moreover, DHA inhibits GluK2(R) with similar onset and recovery kinetics at both negative and positive potentials (Wilding et al., 2005), suggesting that the terminal carboxyl does not enter the pore or experience the membrane potential.

M3 substitutions with uncharged side chains: DHA inhibition and potentiation

The differences we observe between channels with E or D substitutions (Figs. 2 and 3) raise the possibility that steric effects may be more important than charge compensation in determining the interaction between M3 residues and the Q/R site. To test this possibility, we prepared additional mutant subunits with uncharged alanine (A), cysteine (C), or valine (V) substituted at positions T613 through I617 (Fig. 1). As shown in Fig. 4 A, these substitutions had little or no effect on GluK2(Q), which is normally unchanged by DHA

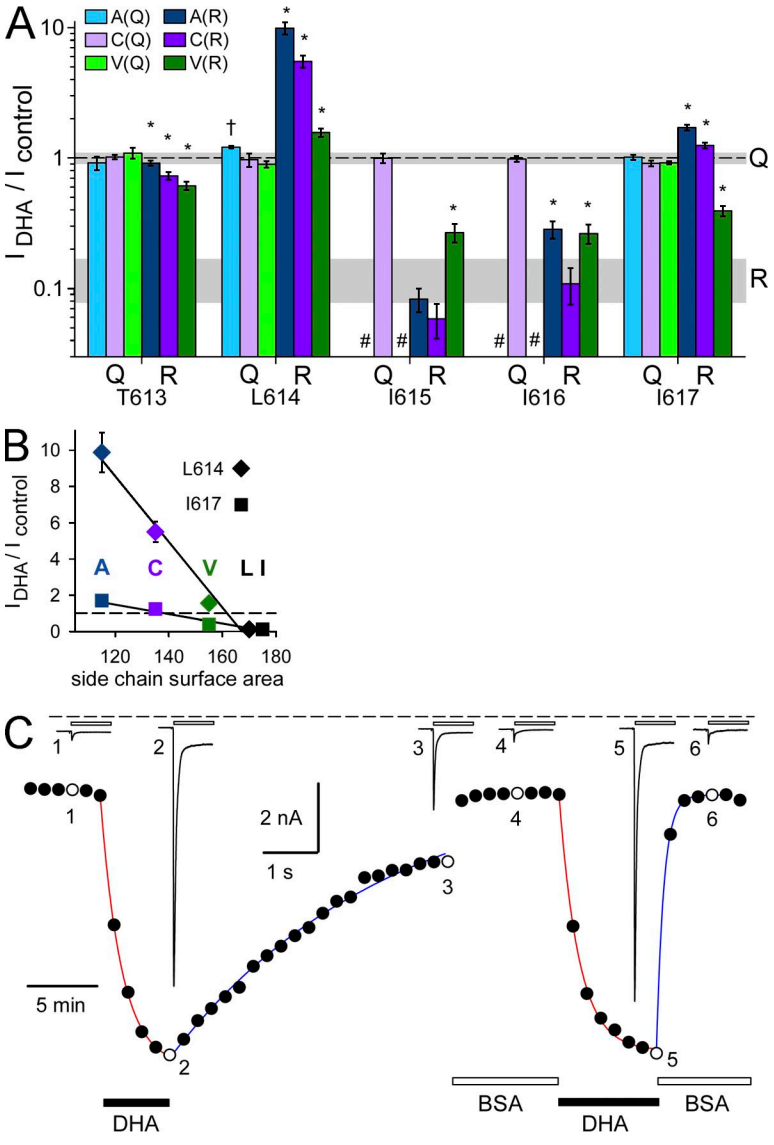

Figure 4. Uncharged M3 substitutions can reverse DHA inhibition of GluK2(R). (A) Plot of steady-state KA-evoked current recorded in Con A–treated cells immediately after exposure to DHA as a fraction of control current before DHA ($I_{DHA}/I_{control}$) for 26 GluK2 substitution mutants (5–29 cells for each construct). Gray horizontal bars centered on 0.12 and 1.0 indicate the 99% confidence intervals for WT GluK2(R) and (Q), respectively. As for WT GluK2(Q), DHA caused minimal change of current evoked through all of the homomeric GluK2(Q) M3 A, C, or V substitutions tested (†, $P < 0.05$; *t* test). In contrast, DHA inhibition of GluK2(R) was reduced or reversed by many of the M3 A, C, or V substitutions (*, $P < 0.05$; *t* test). Loss of DHA inhibition was most prominent for substitutions at T613, L614, or I617 but weaker or absent at I615 and I616. Q590 forms of A and V substitutions at I615 and I616 were not generated (#). (B) $I_{DHA}/I_{control}$ was inversely proportional to side chain surface area for the three uncharged A, C, and V substitutions at L614 ($R = -0.99$) and I617 ($R = -0.978$). The dashed line at 1.0 indicates $I_{DHA} = I_{control}$. (A and B) Results are presented as mean ± SEM. (C) Points plot the peak whole-cell currents evoked by fast application of 300 µM KA in an HEK cell expressing GluK2(R) L614A but not treated with Con A. Closed and open bars below the time course indicate exposure to 15 µM DHA and 0.1% BSA, respectively. Smooth curves are best fits of a single exponential function (in control and BSA, respectively: τ_{on} = 1.5 and 1.4 min [red lines]; τ_{off} = 15.5 and 0.5 min [blue lines]). Sample traces are shown for the six indicated time points.

Published August 12, 2013

exposure (Wilding et al.,2005). In contrast, all of the substitutions yielded some degree of relief from DHA inhibition of GluK2(R). The effect was weakest for I615 and I616, stronger for T613 and I617, and converted to clear potentiation for all three substitutions at L614. Thus, introduction of a charged side chain along M3 is not required for strong and selective modulation of interaction with the Q/R site. However, in contrast to these substantial changes in regulation by DHA, we found that most of the uncharged substitutions were less effective than E or D (Fig. 2) at restoring polyamine block to GluK2(R) (Fig. S4).

As shown in Fig. 4 B, the effect of DHA for the three uncharged substitutions at L614 and I617 was inversely proportional to side chain surface area (correlation coefficients [*R*] were −0.99 and −0.98 for L614 and I617, respectively), suggesting that the local contact surface of residues at these two positions is a determining factor in how DHA alters channel operation. In addition, the fact that points for WT GluK2(R) with L at position 614 and I at position 617 fall along the relationships between $I_{DHA}/I_{control}$ and side chain surface area strongly suggests that the Q/R site interacts with these residues in their native state. Fig. 4 C plots the time course of

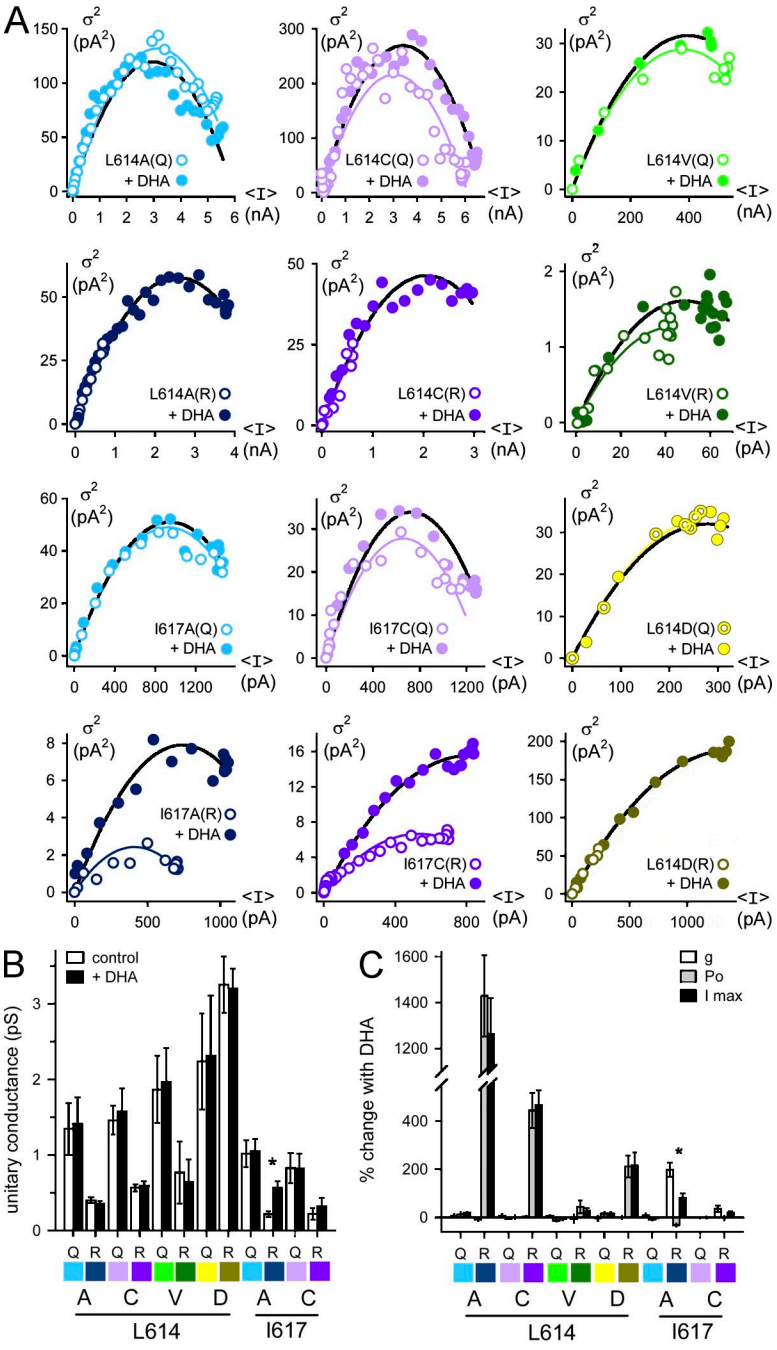

Figure 5. Fluctuation analysis of currents evoked by 10 µM KA in the absence or presence of 15 µM DHA. (A) Plots of current variance (σ^2) versus mean current (<I>) for M3 substitution mutations of GluK2(Q) and (R). The parabolic smooth curves show the best fits of $\sigma^2 = i \times I - I^2/N$, where i is the estimated unitary current amplitude and N is the estimated number of channels. Estimated open probability is given by $P_o = I_{max}/(i \times N)$. (B) Unitary conductance estimated from the variance versus mean fits for three to nine cells for each construct as shown in A. Note that except for the L614D substitution, the Q versus R editing isoforms displayed larger unitary conductance, as observed for WT receptors. Exposure to DHA increased unitary conductance for I617A (*, P = 0.0004) but had no significant effect on conductance for the other substitution mutants. (C) Percent change in conductance, P_o, and I_{max} after DHA exposure shows that larger maximal currents result from increased P_o for substitutions at L614 but from increased unitary current for substitutions at I617 (*, P = 0.0064). Results are presented as mean ± SEM.

Published August 12, 2013

peak current potentiation upon DHA exposure for homomeric GluK2(R) L614A in a cell that was not treated with Con A, illustrating that potentiation did not require elimination of desensitization by Con A preincubation. The onset of potentiation developed along an exponential time course (τ = 1.5 ± 0.5 min, n = 3) and involved minimal change in the kinetics of current activation and desensitization or in the steady-state/peak current ratio. Recovery from potentiation was slow when cells were washed with control saline (τ = 16.4 ± 2.8 min, n = 3) but significantly speeded (τ = 0.84 ± 0.31 min, $P < 0.02$) by inclusion of 0.1% BSA in the wash solution (Wilding et al., 1998).

Fluctuation analysis

To determine whether the changes observed in whole-cell current upon exposure to DHA resulted from alteration in permeation or gating, we used fluctuation analysis to estimate the unitary conductance and open probability for several of the M3 substitution mutants that reduced or reversed the inhibition normally seen for WT GluK2(R). As shown in Fig. 5, for all four of the GluK2(R) L614 substitutions analyzed (A, C, V, and D), exposure to DHA increased the maximal current without a substantial change in the parabolic relation between variance and mean current amplitude. Thus, the action of DHA primarily involved an increase in open probability (Fig. 5, A and C), with no significant change in unitary conductance (Fig. 5, A and B), which is proportional to the initial slope of the variance versus mean plot. In control solution, the (Q) form of these four substitutions had relatively high P_o, which was minimally affected by exposure to DHA (Fig. 5 A). Consistent with the idea that negatively charged side chains substituted along M3 can interact with and neutralize Arg guanidinium groups at the Q/R site, we observed significantly higher estimated unitary conductance for GluK2(R) L614D (Fig. 6 B) and L614E (Fig. S2) than for any of the uncharged substitutions. Thus, D or E substitution at position 614 selectively lowered the energy barrier to cation flux through edited channels, but exposure to DHA did not change the unitary current amplitudes for either the D(R) or E(R) constructs.

In contrast to the L614 substitution mutants, the potentiation observed for GluK2(R) I617A resulted from an increase in unitary conductance, which was also seen to a lesser extent for I617C (note the change in initial slope for I617A(R) and I617C(R) in Fig. 5 A). Interestingly, our earlier analysis (Wilding et al., 2010) showed that potentiation of GluK2(Q) L614R by DHA involves a substantial increase in unitary current and a smaller increase in P_o. Thus, the charge, surface area, and specific position of side chain substitutions along M3 work in combination with the Q/R site residue to determine both unitary current and open probability in control conditions and after treatment with DHA (see Discussion).

Analysis of coupling energies

To compare the strength of pore loop/M3 interactions in GluK2 with previous work on contact surfaces between (Hidalgo and MacKinnon, 1995; Schreiber and Fersht, 1995) and within (Carter et al., 1984) proteins, we used the scheme depicted in Fig. 6 A and K_{eq} values derived from our P_o estimates (Fig. 5) to calculate the coupling energies for individual substitutions with DHA treatment (Fig. 6 B) as well as the coupling between M3 substitutions and Q/R site editing (Fig. 6 C;

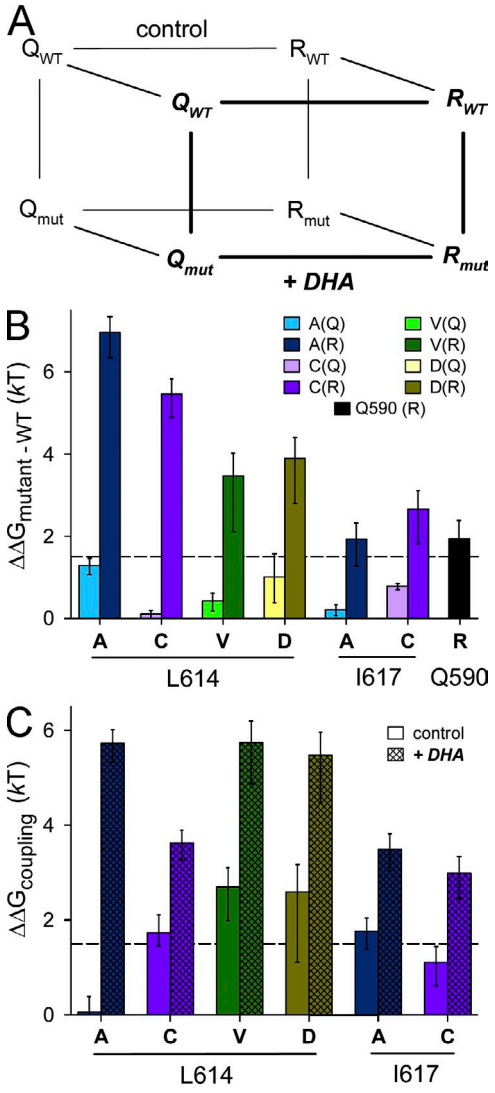

Figure 6. Changes in free energy of channel gating induced by DHA. (A) Diagram of energy cycles for mutant and WT edited and unedited subunits in control solution and with exposure to DHA. (B) $\Delta\Delta G_{mut - WT}$ for the effect of DHA on Q and R forms of each M3 substitution mutant. All substitutions exhibit stronger coupling in the R form than in the Q form. (C) $\Delta\Delta G_{coupling}$ for M3 substitutions and Q/R editing in the absence or presence of DHA. All substitutions exhibit stronger coupling in the presence of DHA than in control conditions, but note that substantial coupling, >1.5 kT, does not require exposure to DHA. The dashed lines at 1.5 kT plot the empirical coupling energy threshold for interacting residues believed to make close contact. Results are presented as mean ± SEM.

Published August 12, 2013

see Materials and methods). Fig. 6 B plots the coupling energies ($\Delta\Delta G_{mut-WT}$) for the left- and right-hand faces of the cubic scheme in Fig. 6 A, allowing comparison of the effect of DHA on substitution mutants of GluK2(Q) and (R), respectively. In each case stronger coupling was observed for M3 substitutions to GluK2(R). For comparison, the black bar in Fig. 6 B plots the coupling energy for Q to R editing, corresponding to the top face of the cubic scheme in Fig. 6 A. As expected, all of these M3 substitutions, which relieve or reverse DHA inhibition of GluK2(R), showed coupling that was equal to or greater than that resulting from Q/R editing alone. Fig. 6 C plots the double mutant cycle coupling energies between M3 mutations and Q/R site editing in the absence (solid bars) or presence (hatched bars) of DHA, which correspond to the back and front faces of the cubic scheme in Fig. 6 A. All of the substitutions exhibit stronger coupling in the presence of DHA; however, it should be noted that even in the absence of DHA, four of the six substitutions exceed coupling energies of ~1.5 *k*T, which was proposed as the empirical cut-off between interactions that involve a direct contact between the two substituted residues ($\Delta\Delta G > 1.5$ *k*T) and those likely to be mediated by indirect allosteric effects ($\Delta\Delta G < 1.5$ *k*T; Schreiber and Fersht, 1995; Ranganathan et al., 1996). Thus, although treatment with DHA substantially increases the apparent coupling between the pore loop and M3 helix, strong coupling does not require DHA exposure (compare with Fig. 2). Importantly, the coupling energies calculated from measurements in control solution (Fig. 6 C, solid bars) do not involve any third variable and thus represent proper double mutant cycles that should indicate the strength of interaction between residues. As noted above for polyamine block, however, we cannot rule out the possibility that coupling energies determined in the presence of DHA reflect changes in the interactions of DHA with each of the substituted residues. If this is the case, it would suggest that strong energetic coupling results from a reduction in interaction with position 614 because the L614D substitution would be expected to repel both the hydrophobic alkene chain and the terminal carboxyl group of DHA.

I-V relations in DHA

In contrast to the significant voltage dependence of GluK2(Q) block by cytoplasmic polyamines (Bowie and Mayer, 1995; Kamboj et al., 1995; Koh et al., 1995), DHA inhibits GluK2(R) equivalently when holding steady at negative and positive membrane potentials with essentially no difference in the rate of onset or recovery from inhibition (Wilding et al., 2005). However, we previously showed that potentiation of currents mediated by homomeric GluK2(Q) L614R after exposure to DHA involves a change in relative permeability to chloride ions (Wilding et al., 2010), with GluK2(Q) L614R being relatively permeable to Cl in control solutions (P_{Cl}/P_{Cs} ~0.5) and exposure to DHA shifting the reversal potential consistent with a nearly 60% reduction in chloride permeability.

To investigate whether DHA affected permeation properties of M3 substitution mutants of GluK2(R), we compared ramp I-V relations for current evoked by KA in control external solution (NaCl), alone or with 15 µM DHA, with the currents recorded in an external solution with nearly all of the chloride replaced by gluconate (see Materials and methods). Among the M3 mutants examined, we observed three different response patterns (Fig. 7 and Table S1). For L614A and C (Fig. 7, A and B), exposure to DHA potentiated current at both negative and positive potentials and reduced chloride permeability as indicated by a rightward shift in reversal potential. For L614V and I617A substitutions (Fig. 7, C and D), the entire I-V relation was shifted to the right such that currents were potentiated at negative potentials (compare with Fig. 4 A) but reduced relative to control at positive potentials. For L614D (Fig. 7 E), currents were potentiated by DHA at all potentials with little or no change in reversal potential and minimal evidence for chloride permeability in these mutants when external chloride was replaced with gluconate. As previously described (Burnashev et al., 1996; Wilding et al., 2010), WT GluK2(R) displayed finite chloride permeability; exposure to DHA inhibited current at all potentials (Wilding et al., 2005) but with only a slight change in reversal potential (Fig. 7 F). Together, these results show that in many cases chloride permeability decreases with DHA modulation, possibly via movement of positive charges away from the central axis of the pore (see below; Wilding et al., 2010); however, a substantial reduction in chloride permeability is not necessary for either potentiation or inhibition by DHA.

DISCUSSION

Collectively, our results provide evidence that editing at the Q/R site substantially alters interaction between the pore loop and side chains along an adjacent segment of the M3 helix and that exposure to DHA increases the strength of this interaction specifically for edited subunits. The results also highlight a significant transition from M3 residues directly adjacent to the pore loop approximately up to the level of T613, where most substitutions produced only partial reductions in DHA inhibition of GluK2(R), and locations at the level of the central cavity including L614, I617, and S618, where complete reversal of the effect of DHA was observed. Our energy calculations are consistent with the possibility of direct interaction between R590 and several of the residues along M3. At many locations, the $\Delta\Delta G$ values exceeded 1.5 *k*T, an energy level which is typically observed for interactions known to involve

Published August 12, 2013

direct contact from independent structural information (Schreiber and Fersht, 1995); however, several factors suggest that values >1.5 *k*T may not be absolutely conclusive in the present case. First, as noted above, the coupling energies determined from polyamine block and DHA modulation may reflect polyamine or DHA interacting with the two substituted positions and not a direct interaction between the two residues. However, this concern should not apply to coupling determined from open probability in the absence of DHA. Second,

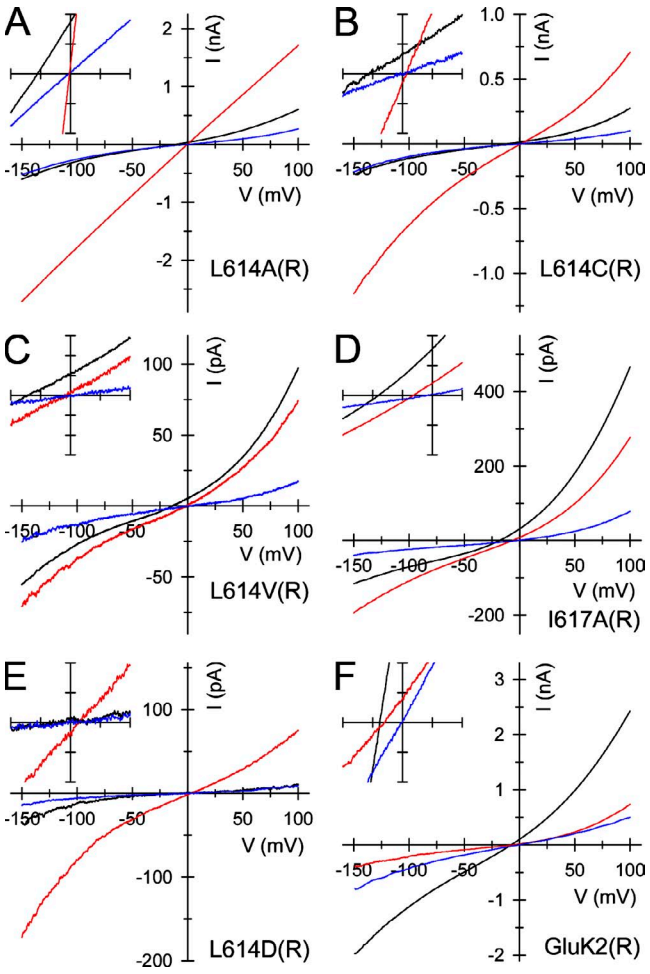

Figure 7. I-V relations in DHA. (A–F) Whole-cell currents were elicited by KA between −150 and 100 mV as membrane potential was ramped at 0.75 mV/ms in control external solution (NaCl) before (black) and after (red) exposure to 15 µM DHA. After recovery from DHA, KA-evoked current was recorded using extracellular Na glucuronate (blue). DHA increased inward and outward current and shifted reversal potentials to the right for GluK2(R) L614A (A) and L614C (B; insets −20 to 20 mV and −40 to 40 pA) and shifted the entire I-V to the right for GluK2(R) L614V (C; inset −20 to 20 mV and −15 to 15 pA) and I617A (D; inset −30 to 10 mV and −40 to 40 pA). (E) GluK2(R) L614D showed little change in reversal potential with either DHA exposure or glucuronate substitution for chloride (inset −20 to 20 mV and −10 to 10 pA). (F) WT GluK2(R) was inhibited by DHA at negative and positive potentials with little change in reversal potential (inset −20 to 20 mV and −40 to 40 pA).

the ΔΔG for coupling between DHA and Q590R editing exceeds 1.5 *k*T (Fig. 6 B, black bar), so that any mutation able to prevent DHA from interacting with the channel should exhibit a double mutant coupling energy change of similar magnitude. The fact that several of the substitutions analyzed in Figs. 5 and 6 do not just eliminate inhibition by DHA but convert it to potentiation demonstrates that a simple mechanism involving loss of the DHA binding does not apply. Instead, the M3 substitutions are likely to alter channel function by changing the conformation and/or interactions of the arginine side chains within edited channels. Third, the surprisingly high values for estimated coupling energies in many of our constructs may reflect the fact that all of our energy calculations were performed for homomeric channels that include four mutated/edited subunits. Yet even if we assume that each subunit only contributes a quarter of the total coupling energy, it is still the case that for many of our M3 substitutions paired with GluK2(R) the estimated contribution for each individual subunit would be >1.5 *k*T, which does support the suggestion of direct contact with the Q/R site. If there is any asymmetry in the open state, such that A/C and B/D subunit pairs do not contribute equivalently, then the energy values for the more strongly coupled subunits would be even larger than if all four are equivalent (see below). Finally, our GluK2(R) homology model (Wilding et al., 2010) based on the closed state crystal structure of the GluA2 AMPA receptor (Sobolevsky et al., 2009) predicts an 8–12-Å separation between R590 and L614, which if correct suggests a significant movement would be needed to bring them into contact in the open state. Such large movements may be tolerated in iGluR channels, which do not need to maintain the very narrow selectivity filter observed in potassium channels that imposes single file passage of K ions while excluding Na and other ions (Doyle at al., 1998).

Fig. 8 A shows a cross section through the transmembrane domain (TMD) of our model (Wilding et al., 2010) viewed from the extracellular side looking in toward the pore loop with residues L614 and I617 displayed as semitransparent cyan and orange spheres, respectively. In the closed state (depicted), both residues are on the side of the M3 helix facing the pore (compare with Fig. 1 B), but neither side chain aims directly at the central axis. Instead, L614 points clockwise around the pore toward the I617 residue on the adjacent subunit. This orientation seems likely to be correct based on the high degree of amino acid identity between GluK2 and GluA2 along nearly the entire length of the M3 helix (Fig. 8 B). In addition, the homologous L606 and I609 residues of GluA1, when substituted with cysteine, can be modified by 2-aminoethyl methanethiosulfonate (Sobolevsky et al., 2003), confirming that they are accessible to the pore. In contrast, the relative location of the Q/R site residue is much less

Published August 12, 2013

certain because there was only weak electron density for side chains along M2 in the crystal structure and even the Cα backbone for most residues in the selectivity filter was not resolved (Sobolevsky et al., 2009). Whether this disorder of the selectivity filter reflects the existence of multiple discrete conformations or more continuous intrinsic mobility of this segment within functional iGluR channels is not known. Fig. 8 A actually shows two possible orientations for the Q/R site Arg side chain because we constrained the A/C and B/D subunits to be symmetric throughout the model but did not impose local fourfold symmetry within the TMD.

Although the conformation of the open state is not known, our combined results (Wilding et al., 2010; this study) suggest that channel opening may involve a clockwise rotation of the M3 helix as viewed from the extracellular domain in Fig. 8 A (Perozo et al., 1999; Flynn et al., 2001), bringing the residue at position 614 closer to the central axis, thus facilitating closer contact with Arg at the Q/R site and accounting for the strong effects on chloride permeability observed for substitutions at this location (Fig. 7), including GluK2(Q) L614R (Wilding et al., 2010). If DHA acts on the channel to oppose this rotation or to reorient M3 in the agonist bound state, then differences in the ability of the local contact surface to interact with and/or accommodate the Arg guanidinium group might explain the change from strong inhibition of GluK2(R) with WT M3 residues to strong potentiation with the various substitution mutants. Although DHA modulation produces an apparent increase in unitary conductance for several M3 substitutions, which could involve a localized change in energy barriers for ion passage along the conduction pathway, for other M3 substitutions, the effect on macroscopic current amplitude can be attributed almost entirely to a change in open probability, possibly suggesting a more global change in subunit conformation that is nevertheless specific to edited channels. Importantly, even in the absence of DHA, the homomeric channels formed by GluK2(R) L614D (Fig. 5 B) and L614E (Fig. S2) exhibit substantially higher estimated unitary conductance than WT GluK2(R) or the subunits with L614 replaced by uncharged side chains, suggesting that electrostatic neutralization significantly enhances cation flux independent of DHA. Moreover, the L614D substitution, which reduces side chain surface area at this position, yielded potentiation with DHA exposure via an increase in open probability. In contrast, channels with L614E substitution, which increases the side chain surface area, were inhibited, on average, to nearly the same extent as WT GluK2(R) (Fig. 3), suggesting that steric accommodation of the Q/R site Arg side chains underlies the changes in gating. Clearly, complete resolution of these possibilities will require more information about the open state conformation of iGluR channels, and for this reason we did

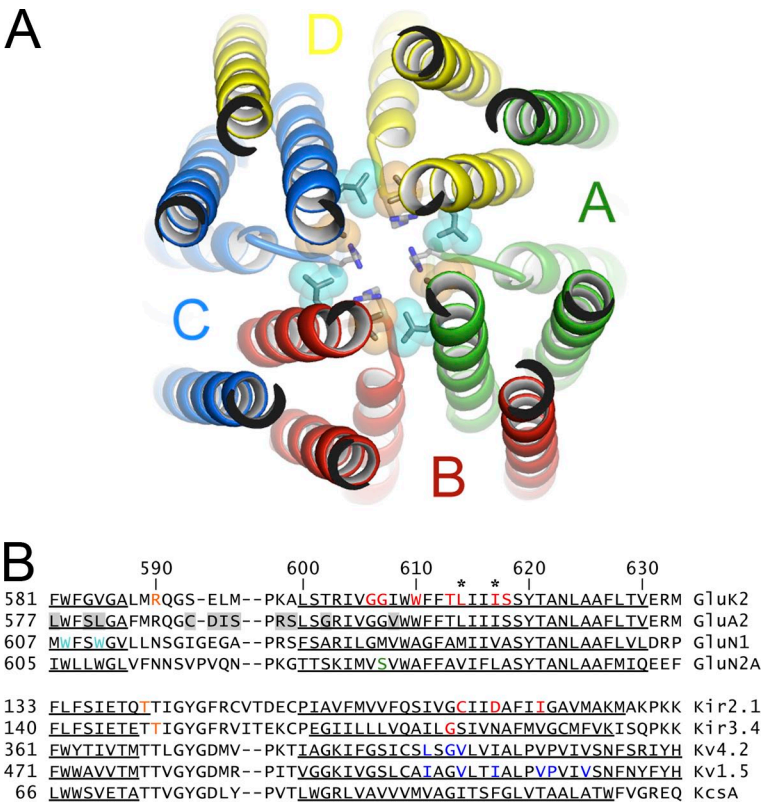

Figure 8. M3 locations strongly interacting with the Q/R site point away from the closed state central axis. (A) Cross section through the pore of our closed state GluK2(R) homology model viewed from the extracellular domain. Portions of the TMD between the two dashed lines in Fig. 1 B are visible. Residues Q590R, L614, and I617 are shown for each subunit, with semitransparent spheres for the side chains of L614 (cyan) and I617 (orange). (B) Partial sequence alignment for the selectivity filter and inner helix segments of KA receptor subunit GluK2(R) (P42260), AMPA receptor subunit GluA2(R) (P19491), NMDA receptor subunits GluN1 (P35439) and GluN2A (Q00959), and subunits of five potassium channels including Kir2.1 (35561), Kir3.4 (P48544), Kv4.2 (Q63881), Kv1.5 (P22460), and KcsA (P0A334). Presumed α helical segments are underlined. Colors indicate interactions between locations in the pore loop (orange) and inner helix (red) of homomeric channels, between the pore helix (cyan) and inner helix (green) of adjacent NMDA receptor subunits, or locations along the inner helix of Kv4.2 and Kv1.5 proposed to interact with AA (blue). Asterisks indicate the location of L614 and I617. GluA2 amino acid residues that are not identical to GluK2 are shaded gray.

Published August 12, 2013

not undertake detailed electrostatic free energy calculations (see below) that might yield additional insights once an open state structure is available.

In addition to our analysis of KA receptors, previous studies of other members of the superfamily have also provided evidence for interaction between the transmembrane inner helix and residues near the tip of the pore loop (Fig. 8 B). For example, current flow through inwardly rectifying Kir2.1 channels with Arg or Lys replacing the native Thr141 (homologous to M589 in GluK2) requires the presence of negative charge in the central cavity supplied by the native Asp172 residue. Kir2.1 T141K or R channels lose function when Asp172 is substituted with an isosteric neutral residue, but activity can be restored by Glu or Asp substitution for C169 or I176 one turn of the helix below or above position 172 (Chatelain et al., 2005). A similar form of electrostatic compensation was observed in work on K_{2P} potassium channels (Kollewe et al., 2009), and in this case, it was shown that swapping the location of the paired charged residues yielded roughly the same level of channel function. Moreover, the work on K_{2P} channels and on a linked K_{2P} tandem tetramer (Kollewe et al., 2009) demonstrated similar levels of electrostatic compensation between pore loop and inner helix charged residues substituted on the same subunit or on adjacent subunits but not on the subunit arranged diagonally across the pore. Finally, in Kir3.4 (GIRK) channels, steric clash between Thr149 (homologous to the Q/R site) and large side chains substituted at a conserved inner helix glycine residue (Gly175) is thought to underlie the reduction in current through homomeric channels formed by these mutant subunits (Chatelain et al., 2005; Rosenhouse-Dantsker and Logothetis, 2006, 2007; Kollewe et al., 2009).

Substitution with a positively charged K or R side chain at the tip of the pore loop in Kir2.1 channels reduced barium block but did not alter relative permeability to monovalent cations or prevent inward rectification by cytoplasmic polyamines (Chatelain et al., 2005), and, as mentioned above, channel function was blocked without a negative counter charge in the central cavity. In contrast, homomeric edited GluK2(R) channels are functional, exhibit novel permeability to chloride as well as monovalent cations (Burnashev et al., 1996), and are not blocked by polyamines (Bowie and Mayer, 1995; Kamboj et al., 1995; Koh et al., 1995). Addition of negative charge in the central cavity reduces chloride permeability of GluK2(R) and increases inward rectification, indicating a partial restoration of polyamine block. The inverted topology and larger minimal pore diameter of iGluR channels (7.5 vs. ~3 Å) are likely to underlie these differences. Cytoplasmic polyamines enter K^+ channels through the open bundle crossing but permeate through the narrow selectivity filter of K^+ channels very slowly, if at all. In contrast, access to iGluR channels involves entry from the pore loop selectivity filter side, and the restoration of outward current flow with strong depolarization is interpreted as relief of block by polyamine permeation (Bähring et al., 1997). Addition of negatively charged residues along the M3 helix of GluK2(R) channels apparently enables entry and increased dwell time of polyamines within the pore; and, swapping the position of the charges preserves this effect.

As for NMDA (Miller et al., 1992) and KA (Wilding et al., 1998) receptors, many potassium channels are susceptible to modulation by cis-unsaturated fatty acids (Boland and Drzewiecki, 2008). Fluorescence quenching and electron paramagnetic resonance studies (Bolivar et al., 2012; Smithers et al., 2012) of fatty acid interaction with reconstituted KcsA channels have detected annular interactions around the channel perimeter as well as nonannular binding at the interface between subunits where anionic phospholipids also bind (Valiyaveetil et al., 2002). In addition, these studies provide evidence for fatty acid entry into the central cavity (Bolivar et al., 2012; Smithers et al., 2012). Recent work on voltage-gated K^+ channels of the Kv4 family suggests that inhibition by AA involves an interaction with the S4-S5 linker region and residues along the inner and outer helices facing away from the pore (Heler et al., 2013). In contrast, experiments on Shaker family K^+ channels indicate that substitutions at several sites along the pore-facing side of the inner helix can reduce inhibition by AA (Decher et al., 2010), including an Ile to Val substitution mediated by RNA editing of Kv1.1. This I to V substitution also speeds recovery of Kv1.1 from N-type inactivation (Gonzalez et al., 2011), leading to the suggestion that both AA (Decher et al., 2010) and the N-terminal inactivation domain (Gonzalez et al., 2011) directly interact with the residue at this position, which is homologous to I617 in GluK2 as well as D172 in Kir2.1 (Fig. 8 B). A scan of Kv1.5 identified at least six inner helix locations where inhibition by 10 µM AA was substantially reduced or eliminated by Ala substitution for Ile, Val, or Pro (Decher et al., 2010), suggesting the contact surface for interaction with AA extends along several inner helix turns.

Thus, at least three possible mechanisms for how DHA modulation of GluK2(R) channels is modified by substitutions at L614, I617, and/or S618 must be considered. First, if DHA were to enter through the bundle crossing and bind directly in the central cavity as proposed for fatty acid inhibition of Kv1.1 and 1.5 (Decher et al., 2010), then substitution with smaller residues at L614 and I617 might provide additional space for DHA to bind and convert steric inhibition of WT GluK2(R) into allosteric potentiation for the A, C, and V substitution mutants. This possibility seems unlikely because it would not explain the similar levels of potentiation we observe for L614D and S618D substitutions, which

Published August 12, 2013

should strongly reduce fatty acid binding along the inner walls of the cavity. In addition, entry of the fatty acid carboxyl group along the ion permeation pathway would be expected to be significantly voltage dependent, which is not observed for inhibition of WT receptors or potentiation of many of the M3 mutants. Alternately, if there is direct contact in the open state between arginine side chains from the Q/R site and regions along the walls of the central cavity formed in large part by the leucines at position 614, then substitutions with smaller and/or negatively charged side chains might better accommodate the four positive guanidinium groups either by electrostatic compensation (Chatelain et al., 2005; Kollewe et al., 2009) in the case of M3 substitutions with Glu and Asp or simply by expanding the cavity volume in the case of uncharged Ala, Cys, and Val. In this scenario, DHA would likely act somewhere outside of the central cavity by an allosteric mechanism that alters the relative motion of the pore loop to accentuate the Q/R site interaction with M3. A third possibility is that DHA may act by partitioning into the membrane and interacting with the TMD along the interface between adjacent subunits (Bolivar et al., 2012) or, possibly, by changing membrane mechanical properties (Patel et al., 2001; Bruno et al., 2007). In this case, M3 substitutions with smaller side chains might alter the allosteric effect of DHA, possibly by opening or enlarging lateral fenestrations that have been observed in several recent channel crystal structures (Payandeh et al., 2011; Brohawn et al., 2012; Miller and Long, 2012), including homomeric GluA2 (Sobolevsky et al., 2009; Mayer, 2011), and have been proposed to allow greater access to the pore by hydrophobic modulators, including fatty acids (Patel et al., 2001). Finally, we cannot entirely rule out the possibility that DHA acts via two independent mechanisms with inhibition caused by DHA binding within the pore and potentiation by a second type of interaction outside of the pore.

KA receptor–mediated whole-cell currents in cultured rat hippocampal neurons are inhibited by AA and DHA (Wilding et al., 1998). As for neuronal receptors in vivo, the receptors present on neurons in dissociated cultures are likely to be heteromeric combinations that include both edited and unedited subunits (Roche and Huganir, 1995; Wilding and Huettner, 2001; unpublished data). Although recombinant WT receptors expressed in heterologous cells only exhibit strong inhibition when all subunits are edited (Wilding et al., 2005), our experiments on homomeric channels providing evidence for interaction between the pore loop Q/R site residue and side chains along the inner helix are likely to be relevant to understanding the operation and modulation of native receptors. As mentioned above, however, our results do not reveal whether these interactions are fourfold symmetric or whether there is any difference or asymmetry between the A/C and B/D subunit pairs in the open state (Payandeh et al., 2012). In addition, our results to date cannot determine whether the interactions occur within individual subunits or between different subunits in the tetramer. The work on K_{2P} channels described above has documented electrostatic compensation between the pore loop of one subunit and inner helix residues either on the same subunit or on adjacent subunits (Kollewe et al., 2009). In addition, a compelling recent study of NMDA receptors (Siegler Retchless et al., 2012) presents evidence for intersubunit interaction between residues along the M2 helix of GluN1 and a serine at the position in M3 of GluN2 that is homologous to G607 in GluK2 (Fig. 8 B). Our ongoing work is now focused on resolving these questions of open state symmetry and within versus between subunit interactions in the pore of GluK2.

We are grateful Mark Mayer for cDNA constructs, Aiwu Lu for technical assistance, and Colin Nichols and Sunjoo Lee for helpful comments on the manuscript.

This work was supported by grants from the National Institutes of Health (NS30888 to J.E. Huettner and GM083914 to M.N. Lopez).

Christopher Miller served as editor.

Submitted: 2 April 2013
Accepted: 11 July 2013

REFERENCES

Bähring, R., D. Bowie, M. Benveniste, and M.L. Mayer. 1997. Permeation and block of rat GluR6 glutamate receptor channels by internal and external polyamines. *J. Physiol.* 502:575–589. http://dx.doi.org/10.1111/j.1469-7793.1997.575bj.x

Boland, L.M., and M.M. Drzewiecki. 2008. Polyunsaturated fatty acid modulation of voltage-gated ion channels. *Cell Biochem. Biophys.* 52:59–84. http://dx.doi.org/10.1007/s12013-008-9027-2

Bolivar, J.H., N. Smithers, J.M. East, D. Marsh, and A.G. Lee. 2012. Multiple binding sites for fatty acids on the potassium channel KcsA. *Biochemistry.* 51:2889–2898. http://dx.doi.org/10.1021/bi300153v

Bowie, D., and M.L. Mayer. 1995. Inward rectification of both AMPA and kainate subtype glutamate receptors generated by polyamine-mediated ion channel block. *Neuron.* 15:453–462. http://dx.doi.org/10.1016/0896-6273(95)90049-7

Bowie, D., G.D. Lange, and M.L. Mayer. 1998. Activity-dependent modulation of glutamate receptors by polyamines. *J. Neurosci.* 18:8175–8185.

Brohawn, S.G., J. del Mármol, and R. MacKinnon. 2012. Crystal structure of the human K2P TRAAK, a lipid- and mechano-sensitive K+ ion channel. *Science.* 335:436–441. http://dx.doi.org/10.1126/science.1213808

Bruno, M.J., R.E. Koeppe II, and O.S. Andersen. 2007. Docosahexaenoic acid alters bilayer elastic properties. *Proc. Natl. Acad. Sci. USA.* 104:9638–9643. http://dx.doi.org/10.1073/pnas.0701015104

Burnashev, N., H. Monyer, P.H. Seeburg, and B. Sakmann. 1992. Divalent ion permeability of AMPA receptor channels is dominated by the edited form of a single subunit. *Neuron.* 8:189–198. http://dx.doi.org/10.1016/0896-6273(92)90120-3

Burnashev, N., A. Villarroel, and B. Sakmann. 1996. Dimensions and ion selectivity of recombinant AMPA and kainate receptor channels and their dependence on Q/R site residues. *J. Physiol.* 496:165–173.

Carter, P.J., G. Winter, A.J. Wilkinson, and A.R. Fersht. 1984. The use of double mutants to detect structural changes in the active site of the tyrosyl-tRNA synthetase (*Bacillus stearothermophilus*). *Cell.* 38:835–840. http://dx.doi.org/10.1016/0092-8674(84)90278-2

Chatelain, F.C., N. Alagem, Q. Xu, R. Pancaroglu, E. Reuveny, and D.L. Minor Jr. 2005. The pore helix dipole has a minor role in inward rectifier channel function. *Neuron.* 47:833–843. http://dx.doi.org/10.1016/j.neuron.2005.08.022

Decher, N., A.K. Streit, M. Rapedius, M.F. Netter, S. Marzian, P. Ehling, G. Schlichthörl, T. Craan, V. Renigunta, A. Köhler, et al. 2010. RNA editing modulates the binding of drugs and highly unsaturated fatty acids to the open pore of Kv potassium channels. *EMBO J.* 29:2101–2113. http://dx.doi.org/10.1038/emboj.2010.88

Dingledine, R., R.I. Hume, and S.F. Heinemann. 1992. Structural determinants of barium permeation and rectification in non-NMDA glutamate receptor channels. *J. Neurosci.* 12:4080–4087.

Doyle, D.A., J. Morais Cabral, R.A. Pfuetzner, A. Kuo, J.M. Gulbis, S.L. Cohen, B.T. Chait, and R. MacKinnon. 1998. The structure of the potassium channel: molecular basis of K+ conduction and selectivity. *Science.* 280:69–77. http://dx.doi.org/10.1126/science.280.5360.69

Eswar, N., D. Eramian, B. Webb, M.Y. Shen, and A. Sali. 2008. Protein structure modeling with MODELLER. *Methods Mol. Biol.* 426:145–159. http://dx.doi.org/10.1007/978-1-60327-058-8_8

Flynn, G.E., J.P. Johnson Jr., and W.N. Zagotta. 2001. Cyclic nucleotide-gated channels: shedding light on the opening of a channel pore. *Nat. Rev. Neurosci.* 2:643–651. http://dx.doi.org/10.1038/35090015

Gonzalez, C., A. Lopez-Rodriguez, D. Srikumar, J.J. Rosenthal, and M. Holmgren. 2011. Editing of human K(V)1.1 channel mRNAs disrupts binding of the N-terminus tip at the intracellular cavity. *Nat Commun.* 2:436–441. http://dx.doi.org/10.1038/ncomms1446

Greger, I.H., L. Khatri, X. Kong, and E.B. Ziff. 2003. AMPA receptor tetramerization is mediated by Q/R editing. *Neuron.* 40:763–774. http://dx.doi.org/10.1016/S0896-6273(03)00668-8

Heler, R., J.K. Bell, and L.M. Boland. 2013. Homology model and targeted mutagenesis identify critical residues for arachidonic acid inhibition of Kv4 channels. *Channels (Austin).* 7:74–84. http://dx.doi.org/10.4161/chan.23453

Hidalgo, P., and R. MacKinnon. 1995. Revealing the architecture of a K+ channel pore through mutant cycles with a peptide inhibitor. *Science.* 268:307–310. http://dx.doi.org/10.1126/science.7716527

Hille, B. 2001. Ion Channels of Excitable Membranes. Third edition. Sinauer Associates, Inc., Sunderland, MA. 814 pp.

Howe, J.R. 1996. Homomeric and heteromeric ion channels formed from the kainate-type subunits GluR6 and KA2 have very small, but different, unitary conductances. *J. Neurophysiol.* 76:510–519.

Huettner, J.E. 1990. Glutamate receptor channels in rat DRG neurons: activation by kainate and quisqualate and blockade of desensitization by Con A. *Neuron.* 5:255–266. http://dx.doi.org/10.1016/0896-6273(90)90163-A

Kamboj, S.K., G.T. Swanson, and S.G. Cull-Candy. 1995. Intracellular spermine confers rectification on rat calcium-permeable AMPA and kainate receptors. *J. Physiol.* 486:297–303.

Kato, A.S., E.R. Siuda, E.S. Nisenbaum, and D.S. Bredt. 2008. AMPA receptor subunit-specific regulation by a distinct family of type II TARPs. *Neuron.* 59:986–996. http://dx.doi.org/10.1016/j.neuron.2008.07.034

Koh, D.S., N. Burnashev, and P. Jonas. 1995. Block of native Ca(2+)-permeable AMPA receptors in rat brain by intracellular polyamines generates double rectification. *J. Physiol.* 486:305–312.

Kollewe, A., A.Y. Lau, A. Sullivan, B. Roux, and S.A. Goldstein. 2009. A structural model for K_{2P} potassium channels based on 23 pairs of interacting sites and continuum electrostatics. *J. Gen. Physiol.* 134:53–68. http://dx.doi.org/10.1085/jgp.200910235

Körber, C., M. Werner, J. Hoffmann, C. Sager, M. Tietze, S.M. Schmid, S. Kott, and M. Hollmann. 2007. Stargazin interaction with alpha-amino-3-hydroxy-5-methyl-4-isoxazole propionate (AMPA) receptors is critically dependent on the amino acid at the narrow constriction of the ion channel. *J. Biol. Chem.* 282:18758–18766. http://dx.doi.org/10.1074/jbc.M611182200

Lingle, C.J. 2006. Empirical considerations regarding the use of ensemble-variance analysis of macroscopic currents. *J. Neurosci. Methods.* 158:121–132. http://dx.doi.org/10.1016/j.jneumeth.2006.05.027

Ma-Högemeier, Z.L., C. Körber, M. Werner, D. Racine, E. Muth-Köhne, D. Tapken, and M. Hollmann. 2010. Oligomerization in the endoplasmic reticulum and intracellular trafficking of kainate receptors are subunit-dependent but not editing-dependent. *J. Neurochem.* 113:1403–1415.

Mayer, M.L. 2011. Emerging models of glutamate receptor ion channel structure and function. *Structure.* 19:1370–1380. http://dx.doi.org/10.1016/j.str.2011.08.009

Miller, A.N., and S.B. Long. 2012. Crystal structure of the human two-pore domain potassium channel K2P1. *Science.* 335:432–436. http://dx.doi.org/10.1126/science.1213274

Miller, B., M. Sarantis, S.F. Traynelis, and D. Attwell. 1992. Potentiation of NMDA receptor currents by arachidonic acid. *Nature.* 355:722–725. http://dx.doi.org/10.1038/355722a0

Panchenko, V.A., C.R. Glasser, K.M. Partin, and M.L. Mayer. 1999. Amino acid substitutions in the pore of rat glutamate receptors at sites influencing block by polyamines. *J. Physiol.* 520:337–357. http://dx.doi.org/10.1111/j.1469-7793.1999.t01-1-00337.x

Panchenko, V.A., C.R. Glasser, and M.L. Mayer. 2001. Structural similarities between glutamate receptor channels and $K(^{+})$ channels examined by scanning mutagenesis. *J. Gen. Physiol.* 117:345–360. http://dx.doi.org/10.1085/jgp.117.4.345

Patel, A.J., M. Lazdunski, and E. Honoré. 2001. Lipid and mechano-gated 2P domain K(+) channels. *Curr. Opin. Cell Biol.* 13:422–428. http://dx.doi.org/10.1016/S0955-0674(00)00231-3

Payandeh, J., T. Scheuer, N. Zheng, and W.A. Catterall. 2011. The crystal structure of a voltage-gated sodium channel. *Nature.* 475:353–358. http://dx.doi.org/10.1038/nature10238

Payandeh, J., T.M. Gamal El-Din, T. Scheuer, N. Zheng, and W.A. Catterall. 2012. Crystal structure of a voltage-gated sodium channel in two potentially inactivated states. *Nature.* 486:135–139.

Perozo, E., D.M. Cortes, and L.G. Cuello. 1999. Structural rearrangements underlying K+-channel activation gating. *Science.* 285:73–78. http://dx.doi.org/10.1126/science.285.5424.73

Ranganathan, R., J.H. Lewis, and R. MacKinnon. 1996. Spatial localization of the K+ channel selectivity filter by mutant cycle-based structure analysis. *Neuron.* 16:131–139. http://dx.doi.org/10.1016/S0896-6273(00)80030-6

Roche, K.W., and R.L. Huganir. 1995. Synaptic expression of the high-affinity kainate receptor subunit KA2 in hippocampal cultures. *Neuroscience.* 69:383–393. http://dx.doi.org/10.1016/0306-4522(95)00253-F

Rosenhouse-Dantsker, A., and D.E. Logothetis. 2006. New roles for a key glycine and its neighboring residue in potassium channel gating. *Biophys. J.* 91:2860–2873. http://dx.doi.org/10.1529/biophysj.105.080242

Rosenhouse-Dantsker, A., and D.E. Logothetis. 2007. Potassium channel gating in the absence of the highly conserved glycine of the inner transmembrane helix. *Channels (Austin).* 1:189–197.

Rosenthal, J.J., and P.H. Seeburg. 2012. A-to-I RNA editing: effects on proteins key to neural excitability. *Neuron.* 74:432–439. http://dx.doi.org/10.1016/j.neuron.2012.04.010

Rozov, A., Y. Zilberter, L.P. Wollmuth, and N. Burnashev. 1998. Facilitation of currents through rat Ca^{2+}-permeable AMPA receptor channels by activity-dependent relief from polyamine block. *J. Physiol.* 511:361–377. http://dx.doi.org/10.1111/j.1469-7793.1998.361bh.x

Salussolia, C.L., A. Corrales, I. Talukder, R. Kazi, G. Akgul, M. Bowen, and L.P. Wollmuth. 2011. Interaction of the M4 segment with other transmembrane segments is required for surface expression of mammalian α-amino-3-hydroxy-5-methyl-4-isoxazolepropionic acid (AMPA) receptors. *J. Biol. Chem.* 286:40205–40218. http://dx.doi.org/10.1074/jbc.M111.268839

Schorge, S., and D. Colquhoun. 2003. Studies of NMDA receptor function and stoichiometry with truncated and tandem subunits. *J. Neurosci.* 23:1151–1158.

Schreiber, G., and A.R. Fersht. 1995. Energetics of protein-protein interactions: analysis of the barnase-barstar interface by single mutations and double mutant cycles. *J. Mol. Biol.* 248:478–486.

Shen, M.Y., and A. Sali. 2006. Statistical potential for assessment and prediction of protein structures. *Protein Sci.* 15:2507–2524. http://dx.doi.org/10.1110/ps.062416606

Siegler Retchless, B., W. Gao, and J.W. Johnson. 2012. A single GluN2 subunit residue controls NMDA receptor channel properties via intersubunit interaction. *Nat. Neurosci.* 15:406–413: S1–S2. http://dx.doi.org/10.1038/nn.3025

Sigworth, F.J. 1980. The variance of sodium current fluctuations at the node of Ranvier. *J. Physiol.* 307:97–129.

Smithers, N., J.H. Bolivar, A.G. Lee, and J.M. East. 2012. Characterizing the fatty acid binding site in the cavity of potassium channel KcsA. *Biochemistry.* 51:7996–8002. http://dx.doi.org/10.1021/bi3009196

Sobolevsky, A.I., M.V. Yelshansky, and L.P. Wollmuth. 2003. Different gating mechanisms in glutamate receptor and K^+ channels. *J. Neurosci.* 23:7559–7568.

Sobolevsky, A.I., M.P. Rosconi, and E. Gouaux. 2009. X-ray structure, symmetry and mechanism of an AMPA-subtype glutamate receptor. *Nature.* 462:745–756. http://dx.doi.org/10.1038/nature08624

Sommer, B., M. Köhler, R. Sprengel, and P.H. Seeburg. 1991. RNA editing in brain controls a determinant of ion flow in glutamate-gated channels. *Cell.* 67:11–19. http://dx.doi.org/10.1016/0092-8674(91)90568-J

Swanson, G.T., D. Feldmeyer, M. Kaneda, and S.G. Cull-Candy. 1996. Effect of RNA editing and subunit co-assembly single-channel properties of recombinant kainate receptors. *J. Physiol.* 492:129–142.

Swartz, K.J., W.J. Koroshetz, A.H. Rees, and J.E. Huettner. 1992. Competitive antagonism of glutamate receptor channels by substituted benzazepines in cultured cortical neurons. *Mol. Pharmacol.* 41:1130–1141.

Terhag, J., K. Gottschling, and M. Hollmann. 2010. The transmembrane domain C of AMPA receptors is critically involved in receptor function and modulation. *Front. Mol. Neurosci.* 3:117. http://dx.doi.org/10.3389/fnmol.2010.00117

Traynelis, S.F., L.P. Wollmuth, C.J. McBain, F.S. Menniti, K.M. Vance, K.K. Ogden, K.B. Hansen, H. Yuan, S.J. Myers, and R. Dingledine. 2010. Glutamate receptor ion channels: structure, regulation, and function. *Pharmacol. Rev.* 62:405–496. http://dx.doi.org/10.1124/pr.109.002451

Valiyaveetil, F.I., Y. Zhou, and R. MacKinnon. 2002. Lipids in the structure, folding, and function of the KcsA K+ channel. *Biochemistry.* 41:10771–10777. http://dx.doi.org/10.1021/bi026215y

Wilding, T.J., and J.E. Huettner. 2001. Functional diversity and developmental changes in rat neuronal kainate receptors. *J. Physiol.* 532:411–421. http://dx.doi.org/10.1111/j.1469-7793.2001.0411f.x

Wilding, T.J., Y.H. Chai, and J.E. Huettner. 1998. Inhibition of rat neuronal kainate receptors by cis-unsaturated fatty acids. *J. Physiol.* 513:331–339. http://dx.doi.org/10.1111/j.1469-7793.1998.331bb.x

Wilding, T.J., Y. Zhou, and J.E. Huettner. 2005. Q/R site editing controls kainate receptor inhibition by membrane fatty acids. *J. Neurosci.* 25:9470–9478. http://dx.doi.org/10.1523/JNEUROSCI.2826-05.2005

Wilding, T.J., E. Fulling, Y. Zhou, and J.E. Huettner. 2008. Amino acid substitutions in the pore helix of GluR6 control inhibition by membrane fatty acids. *J. Gen. Physiol.* 132:85–99. http://dx.doi.org/10.1085/jgp.200810009

Wilding, T.J., K. Chen, and J.E. Huettner. 2010. Fatty acid modulation and polyamine block of GluK2 kainate receptors analyzed by scanning mutagenesis. *J. Gen. Physiol.* 136:339–352. http://dx.doi.org/10.1085/jgp.201010442

Lopez et al., http://www.jgp.org/cgi/content/full/jgp.201311000/DC1

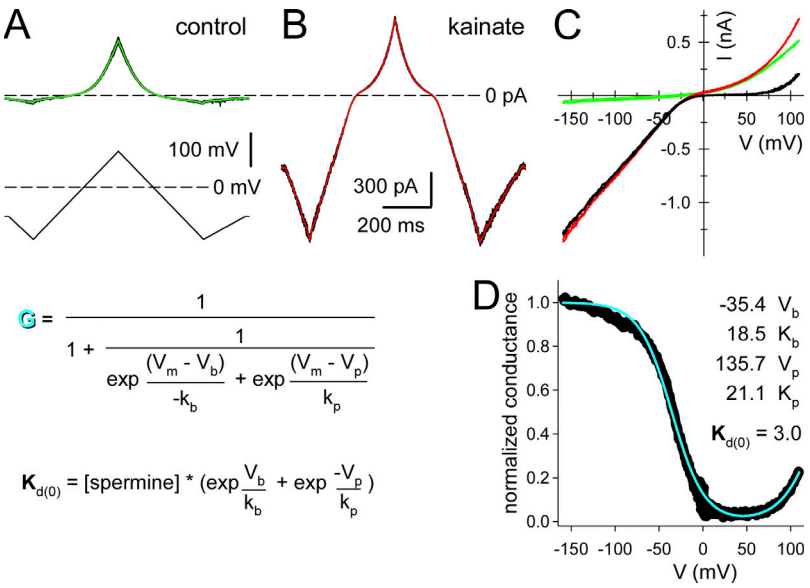

Figure S1. Analysis of polyamine block from I-V relations. (A and B) Whole-cell currents recorded in control (A) or KA-containing (B) extracellular solution during triangle wave ramp stimulation. The voltage command, which was repeated five times, is shown in A below the current recordings. The five individual recordings are shown superimposed as black traces, and the averaged currents are shown in green (A) or red (B). Note that the same current and time scales are used in A and B. (C) Mean current in control (green) or KA-containing (red) external solution during the central ascending and descending ramps is plotted versus command voltage. The black trace shows KA-evoked current obtained by subtracting the green trace from the red trace. Note that the current axis in C is aligned and plotted at the same scale as in A and B and that the currents evoked by the ascending and descending ramps superimpose without any evidence of hysteresis. (D) Normalized conductance versus voltage plot obtained from $G = I/(V_m - V_{rev})$. Note that the voltage axis in D is aligned and plotted at the same scale as in C. A few points have been blanked where G diverges toward $-\infty$ and $+\infty$ near the position when $V_m = V_{rev}$. The smooth cyan curve plots the best fit of the top equation shown to the left of D that describes a voltage-dependent permeant blocker, where the four fit parameters V_b, V_p, k_b, and k_p are the midpoint voltages and slope factors for polyamine block and permeation, respectively. Values of the adjusted parameters for this cell are shown in D as well as the spermine dissociation constant at 0 mV ($K_{d(0)}$) calculated from the fit parameters using the bottom equation shown to the left of D.

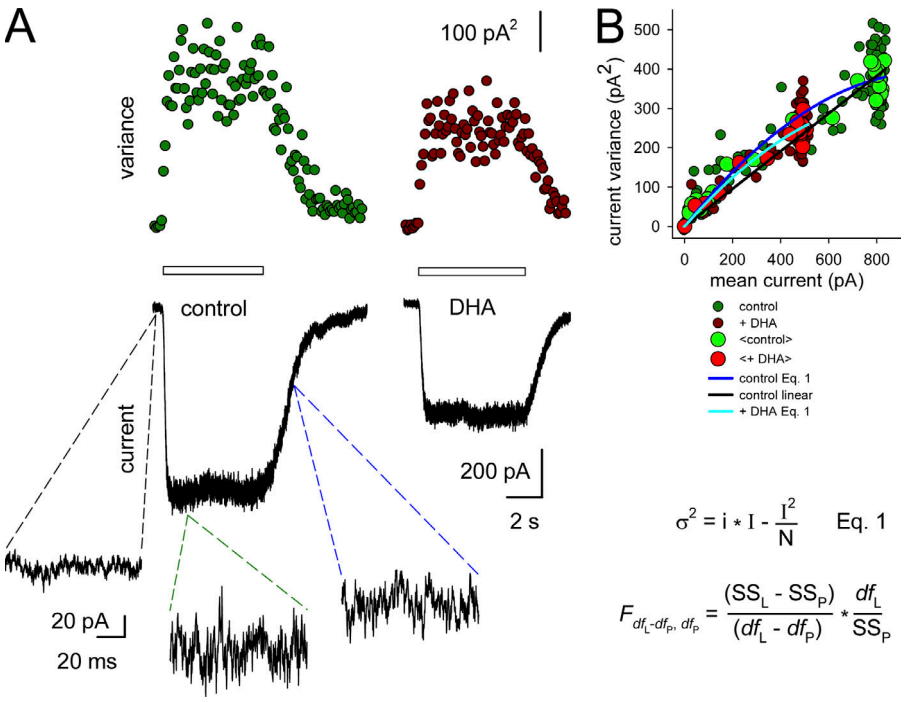

Figure S2. Fluctuation analysis for GluK2(R) L614E. (A) Whole-cell currents evoked by 10 µM KA in the absence or presence of 15 µM DHA are shown below and current variance for 100-ms segments is plotted above each trace. (B) Plots of the KA-evoked increase in current variance (σ^2) versus mean current (<I>) before (control) and immediately after exposure to DHA. Note that the variance axis in B is aligned and plotted at the same scale as in A. Small symbols plot the individual (mean, variance) pairs; larger symbols plot means of five adjacent (mean, variance) pairs. The parabolic smooth curves show the best fits of Eq. 1, $\sigma^2 = i \times I - I^2/N$, to the individual (mean, variance) pairs, where N is the estimated number of channels (2,671 for the control fit) and i is the estimated unitary current amplitude (0.77 pA for the control fit). At −80 mV, the unitary current for this cell corresponds to a unitary conductance of 9.6 pS, and, on average, the value was 7.10 ± 0.94 pS (n = 17 cells). N was determined from the best fit to the control data points and was then held constant as i was adjusted to fit Eq. 1 to the data in DHA (0.70 pA for DHA). For clarity, only the averaged (mean, variance) pairs are shown in Fig. 5 A. Estimated open probability is given by $P_o = I_{max}/(i \times N)$. Despite the relatively low control P_o (0.41 for control fit; 0.26 for DHA) in this cell, the two-parameter parabola defined by Eq. 1 nevertheless provides a significantly superior fit compared with the best fit straight line through the origin as determined by calculating the ratio of residual deviations (bottom equation; Swartz et al., 1992). For the control plot, $F_{1, 117} = 21$, which is larger than the tabulated value of ∼4 for $\alpha = 0.05$ in the F distribution.

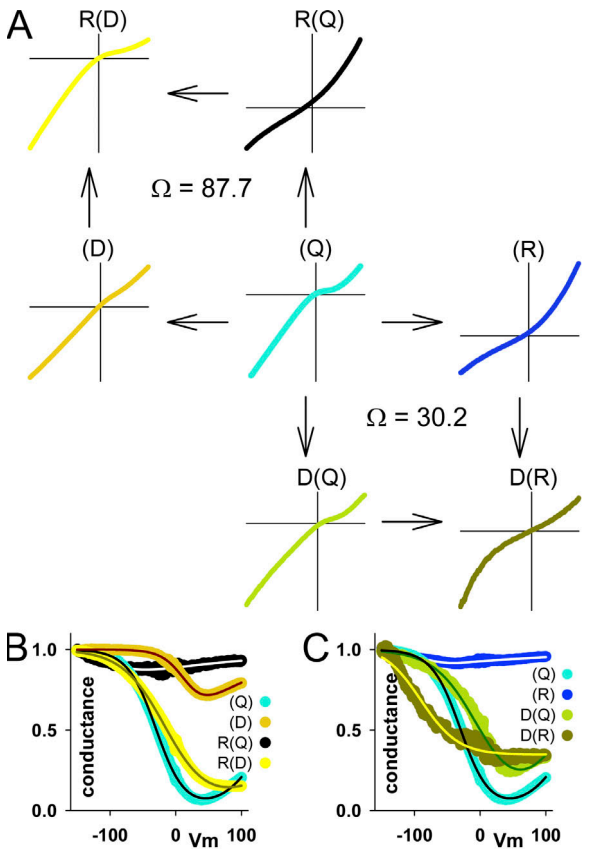

Figure S3. Mutant cycles for R and D substitutions at the Q/R site and at position L614 in the M3 helix. (A) Plots show KA-evoked whole-cell current recorded for WT GluK2(Q) and (R), for GluK2(D), and for substitution mutants at position L614 between −150 and 100 mV during slow voltage ramps (0.75 mV/ms). Bi-rectification of current mediated by GluK2(Q) reflects strong block by endogenous polyamines, as well as 20 µM spermine added to the internal solution, with progressive relief of block as the polyamines permeate the channel at more positive potentials. Q/R site editing or Arg substitution at position 614 eliminates polyamine block. Asp substitution at the Q/R site or position 614 also reduces polyamine block, but inward rectification is partially restored for GluK2(R) L614D and GluK2(D) L614R. (B and C) Normalized conductance versus voltage plots for the constructs in A. Smooth curves are the best fits of $G = 1/(1 + (1/B))$, where $B = \exp(-(V_m - V_b)/k_b) + \exp((V_m - V_p)/k_p)$, where V_b, V_p, k_b, and k_p are the midpoint voltages and slope factors for polyamine block and permeation, respectively (see Materials and methods and Fig. S1 D). Polyamine K_d at 0 mV $K_{d(0)} = [\text{spermine}] \times (\exp(V_b/k_b) + \exp(-V_p/k_p))$ was used to calculate the coupling coefficients: $\Omega = (K_{d\,WT:WT} \times K_{d\,mut1:mut2})/(K_{d\,mut1:WT} \times K_{d\,WT:mut2})$. The coupling coefficients 87.7 and 30.2 indicate coupling energies of 4.5 and 3.1 *k*T for the R(D) and D(R) cycles, respectively, where the Q/R site residue is given in parenthesis (see Fig. 2 D).

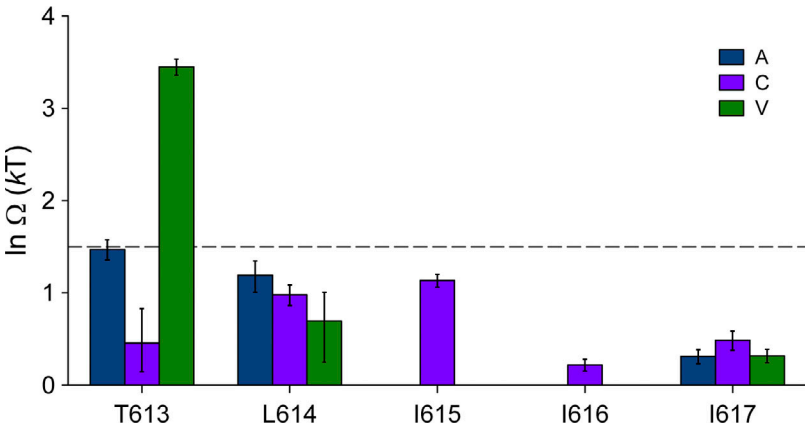

Figure S4. Coupling energies for polyamine block of neutral M3 substitutions. Coupling energies were calculated as $\Delta G = RT \ln\Omega$, where Ω was obtained from analysis of polyamine block in 4–10 cells for each construct as shown in Figs. 2, S1, and S3. The dashed line at 1.5 *k*T plots the empirical coupling energy threshold for interacting residues believed to make close contact. Results are presented as mean ± SEM.

Table S1

Reversal potentials and estimated relative chloride permeability

Construct	V_{rev}			P_{Cl}/P_{Cs}	*n*
	NaCl	NaCl + DHA	Na glucuronate		
	mV	*mV*	*mV*		
GluK2(R)	−7.57 ± 1.61	−6.09 ± 2.58	−0.10 ± 0.72	0.33 ± 0.08	5
L614A(R)	−10.98 ± 1.78	−0.30 ± 0.84	−0.37 ± 0.89	0.50 ± 0.11	5
L614C(R)	−11.14 ± 0.41	1.33 ±1.71	−0.83 ± 3.82	0.48 ± 0.24	3
L614V(R)	−13.90 ± 2.25	−1.82 ± 2.15	0.93 ± 7.22	0.77 ± 0.46	5
L614D(R)	−3.15 ± 2.30	2.90 ± 0.70	0.35 ± 1.00		5
L614E(R)	−1.40 ± 3.10	−1.94 ± 4.01	−4.11 ± 2.01		5
I617A(R)	−18.39 ± 6.06	−6.23 ± 0.67	−2.04 ± 3.01	0.85 ± 0.27	4

REFERENCE

Swartz, K.J., W.J. Koroshetz, A.H. Rees, and J.E. Huettner. 1992. Competitive antagonism of glutamate receptor channels by substituted benzazepines in cultured cortical neurons. *Mol. Pharmacol.* 41:1130–1141.